12,05

Structure and properties of glycine-modified iron oxide nanoparticles for biomedical applications

© A.S. Kamzin[1], I. Kozenkov[2], T. Sviridova[2], V. Rodionova[2], A. Omelyanchik[2]

[1] Ioffe Institute,
St. Petersburg, Russia
[2] Immanuel Kant Baltic Federal University,
Kaliningrad, Russia

E-mail: askam@mail.ioffe.ru

Received September 21, 2025
Revised September 21, 2025
Accepted September 29, 2025

Properties, a structure and sizes of the iron oxide particles produced by co-precipitation in the presence of glycine have been studied in a dependence on an amount of glycine in a reaction mixture from 0.0 mol, 0.1 mol, 0.3 mol and 0.6 mol. It was shown by data of Mossbauer spectroscopy that the synthesized particles are single-phase magnetite spinel ferrite nanoparticles (Fe_3O_4). It is shown by results of X-ray diffraction and Mössbauer studies that with an increase of the glycine concentration (0.1 mol, 0.3 mol and 0.6 mol) the particle sizes decrease from 11 nm, 10 nm and to 6 nm, respectively. The data of the Mössbauer studies of the particles indicate differences of the magnetic structures of a surface layer and a volume of the particles, which significantly affects the nanoparticle properties. An approach for creating special iron oxide nanoparticles has been developed for diagnostics and therapy (theranostics) of human diseases.

Keywords: magnetic nanoparticles, functionalization, magnetic properties, magnetic structure.

DOI: 10.61011/PSS.2025.09.62363.259a-25

1. Introduction

Currently, magnetic nanoparticles (MNP) are intensely studied as promising materials for a wide range of practical applications: catalysts, means for hydrogen productions, purification of waste and air from CO_2, etc. [1,2]. An important field of MNP applications is biomedicine, namely, targeted delivery of drugs straight to a disease hotbed, illness diagnostics, for example, with improving contrast of magnetic-resonance tomography images, cancer treatment with magnetic hyperthermia (MHT) [3–6]. The MHT is based on heating the MNPs placed in a tumor under effect of an external variable magnetic field, as it was shown for the first time in 1957 [7]. When reaching the temperatures of 45 °C, malignant cells die, whereas healthy cells are not damaged [6–8].

A new unique method of Magnetic particle imaging (MPI) of human organs was proposed for disease diagnostics in 2000 [9,10]. The MPI method differs from the known method of visualization by high efficiency, sensitivity and resolution. However, this method imposes rigid requirements to the properties of the magnetic nanoparticles that are sensors or signal indicators in MPI [11–15]. In this regard, the known methods of MNP production and modification of their surface began to develop and new methods thereof began to be created [16–21]. The particles shall be modified or coated in order to eliminate non-specific adsorption of biomolecules, interactions *in vitro* and *in vivo*, relative toxicity and aggregation tendencies since it all prevents practical application of the particles. Typical polymer coatings include organic materials, such as polyethyleneglycol (PEG), polyvinyl alcohol (PVA), poly(N,N-dimethylacrylamide) or inorganic materials, for example, silicon [16].

For biomedical applications, very convenient are the iron oxide magnetic nanoparticles: hematite (α-Fe_2O_3), maghemite (γ-Fe_2O_3) and magnetite (Fe_3O_4), which are the most biologically-compatible as they are present in living organisms. Among the iron oxide magnetic nanoparticles, the most popular for biomedical applications is magnetite (Fe_3O_4) that has many unique properties, such as a small size (< 100 nm) that allows them functioning at a cell level, supermagnetism, high magnetization and a large specific area of the surface. The nanoparticles based on Fe_3O_4 were approved by USA Food and Drug Administration for application in hyperthermia treatment.

There are multiple methods of producing various types of the magnetite MNPs (Fe_3O_4) that differ by a form, morphology, size and availability of reactive groups on the surface [3,16–21]. They include a method of grinding of bulk magnetite together with a surfactant in a ball mill, a hydrothermal method, sol-gel, pyrolysis sputtering, co-precipitation of the salts Fe(III) and Fe(II) in presence of an aqueous base (for example, NH_3OH or NaOH), thermal decomposition of metalorganic complexes in high-boiling solvents, etc. Reduction of the particle size to the nanoscale often results in reduction of saturation magnetization due to dimensionality effects and enhancement of the influence of such a „defect“ as a surface [22,23]. In this regard, it is rele-

vant to search for new MNP synthesis technologies that can control the magnetic properties in order to create functional MNPs for theranostics and probes for visualization.

Glycine-assisted co-precipitation provides a simple and efficient route for simultaneous particle growth control and in situ surface functionalization [20,24]. The MNP synthesis by glycine-modified co-precipitation also attracts attention because glycine is a predecessor of some important metabolites, responsible for protective deceleration processes, reduces psychoemotional stress and improves brain functioning [25].

The aim of the present study was to investigate formability of the iron oxide MNPs under conditions of glycine-modified co-precipitation and to study the influence of the synthesis conditions on a composition, structure, morphology and dimensionality of the MNPs being synthesized. The study is important since it is necessary to create special iron oxide nanoparticles and chemistry of their surface for using both for diagnostics and therapy of human diseases (theranostics).

2. Materials and methods

2.1. Reagents

The following reagent were used for MNP synthesis: iron sulphate (II), hydrate $FeSO_4 \cdot 7H_2O$, iron chloride (III), hydrate $FeCl_3 \cdot 6H_2O$ (manufactured by Neva Reaktiv, Russia), glycine of purity of 97% and sodium hydroxide NaOH (manufactured by Neva Reaktiv, Russia). The materials for synthesis were neither purified nor treated additionally. The particles were flushed using ethanol (C_2H_6O) of purity of $> 99\%$. The solution was prepared by using deionized water. The MNPs were synthesized under conditions of no oxygen.

2.2. Synthesis of the iron oxide MNPs and modification by glycine

The iron oxide MNPs investigated in this study were synthesized by a co-precipitation approach commonly employed for iron oxide MNP preparation [26]. The procedure was modified by introducing glycine, as described in detail in our previous work [20], where some of the samples analyzed here were already reported. In order to produced the iron oxide MNPs, a solution of the two salts $FeSO_4 \cdot 7H_2O$ and $FeCl_3 \cdot 6H_2O$ was prepared in degassed deionized water, in respective quantities (see Table 1). The prepared solution in a 100 ml flask was immersed into a water bath of the room temperature. Then, glycine was added in order to make a required concentration in the reaction solution during the entire reaction time. The produced reaction solution was mixed by a mechanical mixer at a rotational speed of 800 revs/min while heating up to 80 °C. At the mixture temperature of 80 °C NaOH was added by drops and mixing continued for 2 h. Upon completion of this reaction time, the solution was decanted to flush away the particles by ethanol and centrifuged at 2900 revs/min for 10 min. The described procedure was repeated twice and then the particles were separated and dried for 12 h at 70 °C. In order to compare properties of the glycine-modified iron oxide MNPs with properties of the unmodified particles, the iron oxide MNPs without glycine were also prepared. As a result, we have produced the iron oxide MNPs without glycine and those modified with the different glycine concentrations (0.10, 0.30 and 0.60 mol/l), which are hereinafter designated to as M/G0.0, M/G0.1, M/G0.3 and M/G0.6.

Table 1. Used components and their amounts for producing the iron oxide MNPs unmodified and modified with glycine

Sample	$FeSO_4 \cdot 7H_2O$ (mol)	$FeCl_3 \cdot 6H_2O$ (mol)	Glycine (mol)	NaOH (mol)
M/G0.6	0.10	0.20	0.60	3.00
M/G0.3	0.10	0.20	0.30	3.00
M/G0.1	0.10	0.20	0.10	3.00
M/G0.0	0.10	0.20	0	0

3. Experimental procedures

Powder X-ray diffraction (XRD) was performed by means of a diffractometer PW 3040/60 X'Pert Pro Röntgen using Cu K_α radiation ($\lambda = 1.5406$ Å) and a Bragg–Brentano configuration $\theta/2\theta$ at the room temperature within the range $2\theta = 10-80°$. The systems includes a superfast detector PW3015/20 X'Celerator and a secondary monochromator. Bragg reflections of X-ray diffraction patterns were refined and modeled using the software [27]. Equipment broadening was measured using a germanium powder without physical broadening. Accuracy of the lattice parameter was 0.008 Å.

The Mössbauer spectroscopy used in the study makes it possible to specify a structure, phase composition and concentration of the different iron oxides in the studied materials [18–23], which can not be made by other known methods. It is related to significant differences in the properties and the magnetic structure of the iron oxides, which are distinguished by the Mössbauer spectroscopy, which is impossible when using, for example, X-ray diffraction, since values of the lattice constants of the iron oxides are very close.

The Mössbauer spectra (MS) were obtained by means of a Mössbauer spectrometer that is designed to operate in a constant acceleration mode with a triangular form of a velocity of source motion velocity in relation to an absorber. A geometry of transmission of gamma-quanta from the Co-57(Rh) source through the studied sample was used. A velocity scale was calibrated using a metal foil

α-Fe at the room temperature, and values of isomer shifts are provided in relation thereof. The experimental MS obtained at 300 and 80 K were mathematically processed using the software SpectrRelax [28] that used a least-square method and a Lorentz form of spectral lines. The software SpectrRelax [28] makes it possible to extract distributions of parameters of hyperfine interactions (HPI) when using the spectral line of the Voight form.

4. Results and discussion

4.1. X-ray diffraction analysis

The X-ray diffraction patterns of the produced samples are shown in Figure 1 and it should be noted that they similar to those provided in the literature (see, for example, [29–33]). The lines observed in the X-ray images that are refined by Rietveld correspond to the main grating planes (220), (311), (222), (400), (422), (511), (440) and (533) of a single-phase mixed cubic spinel structure with the space group Fd3m. It was shown by the calculations that the lattice parameter α of the lattice cells was 8.361 Å, which is intermediate between the parameters of magnetite ($\alpha = 8.396$ Å, JCPDS №19-0629) and maghemite ($\alpha = 8.346$ Å, JCPDS №39-1346), i. e. it corresponds to a structure of the nonstoichiometric magnetite type ($Fe_{3-x}O_4$) [30]. It can indicate that the produced MNPs include both the iron oxide types. However, the diffraction patterns (Figure 1) have not additional lines in the range $2\Theta \approx 28$ and 30 degreed, which belong to maghemite. Average sizes of the crystallites, which are calculated by the Debye–Scherrer formula, were 6.9 nm for the Fe_3O_4 samples, while with glycine modification M/G0.1, M/G0.3 and M/G0.6 the particle sizes were reduced from 9.4 ± 5 to 6.8 ± 5 nm (Table 2).

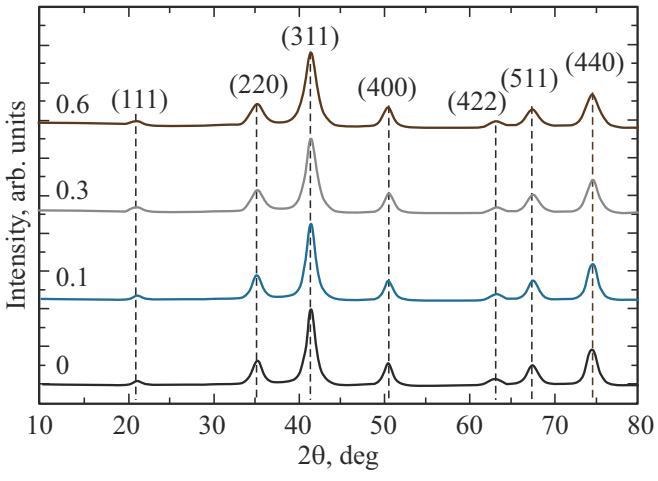

Figure 1. X-ray diffraction patterns of the iron oxide MNPs synthesized at the different glycine concentrations.

Table 2. Results of X-ray diffraction analysis of the MNP samples synthesized at the various glycine concentrations: the lattice parameter (α), the particle size (d_{XRD})

Sample	Glycine (mol)	α (nm)	d_{XRD} (nm)
M/G0/0	0	0.8368	6.9 ± 5
M/G0.1	0.10	0.8360	9.4 ± 5
M/G0.3	0.30	0.8361	8.3 ± 5
M/G0.6	0.60	0.8362	6.8 ± 5

4.2. Mössbauer spectroscopy of the synthesized MNPs

The Mössbauer spectra (MS), recorded at 300 and 80 K, of the samples M/G0.0, M/G0.1, M/G0.3 and M/G0.6 are shown in Figure 2, *a* and Figure 3, *a*, respectively. It should be noted that the obtained experimental Mössbauer spectra (Figure 2 and Figure 3) are similar to iron oxides' spectra published, for example, in [34–48].

When studying the synthesized iron oxides, one of the most important issue is to identify phases in the produced materials. Different methods are used for studying the iron oxide particles of a crystal and a magnetic structure, phase states, size distributions of the particles: X-ray diffraction (XRD), transmission electron microscopy (TEM), the spectroscopic methods (the Mössbauer effect, EXAFS). These methods study the MNPs in various sampling scales. In case of single-domain particles, values of the sizes of the particles produced by the XRD and TEM methods are not comparable, unless the samples are highly-monodisperse (which is hardly possible in real samples). Incomparability is mainly caused by the fact that in case of TEM the average values of the particle sizes are obtained from a limited number of the MNPs (usually 100–300), but when using the XRD or Mössbauer spectroscopy the size distribution is obtained from a much higher number of the particles. Unambiguous identification of the nanometer-scale particles Fe_3O_4 and γ-Fe_2O_3 by the XRD method is almost impossible since the values of crystal lattice constants of these oxides are close ($Fe_3O_4 = 8.397$ A, γ-$Fe_2O_3 = 8.374$ A). When using the Mossbauer spectroscopy for studying the particles that simultaneously include Fe_3O_4 and γ-Fe_2O_3, at the MNP sizes below 10 nm we observe a superparamagnetic relaxation effect that results in broadening and overlapping of the absorption lines, thereby significantly deteriorating the MS spectral lines and complicating their analysis [22].

Processing of the experimental MS of the MNPs M/Gl was based on the following facts: in Fe_3O_4 the ions Fe^{2+} occupy a half of the positions of the octahedral B-sublattice, while the ions Fe^{3+} are uniformly distributed over the tetrahedral A-positions and the remaining half of the octahedral B-positions [22]. Consequently, the magnetite MS shall include three Zeeman sextuplets that are induced

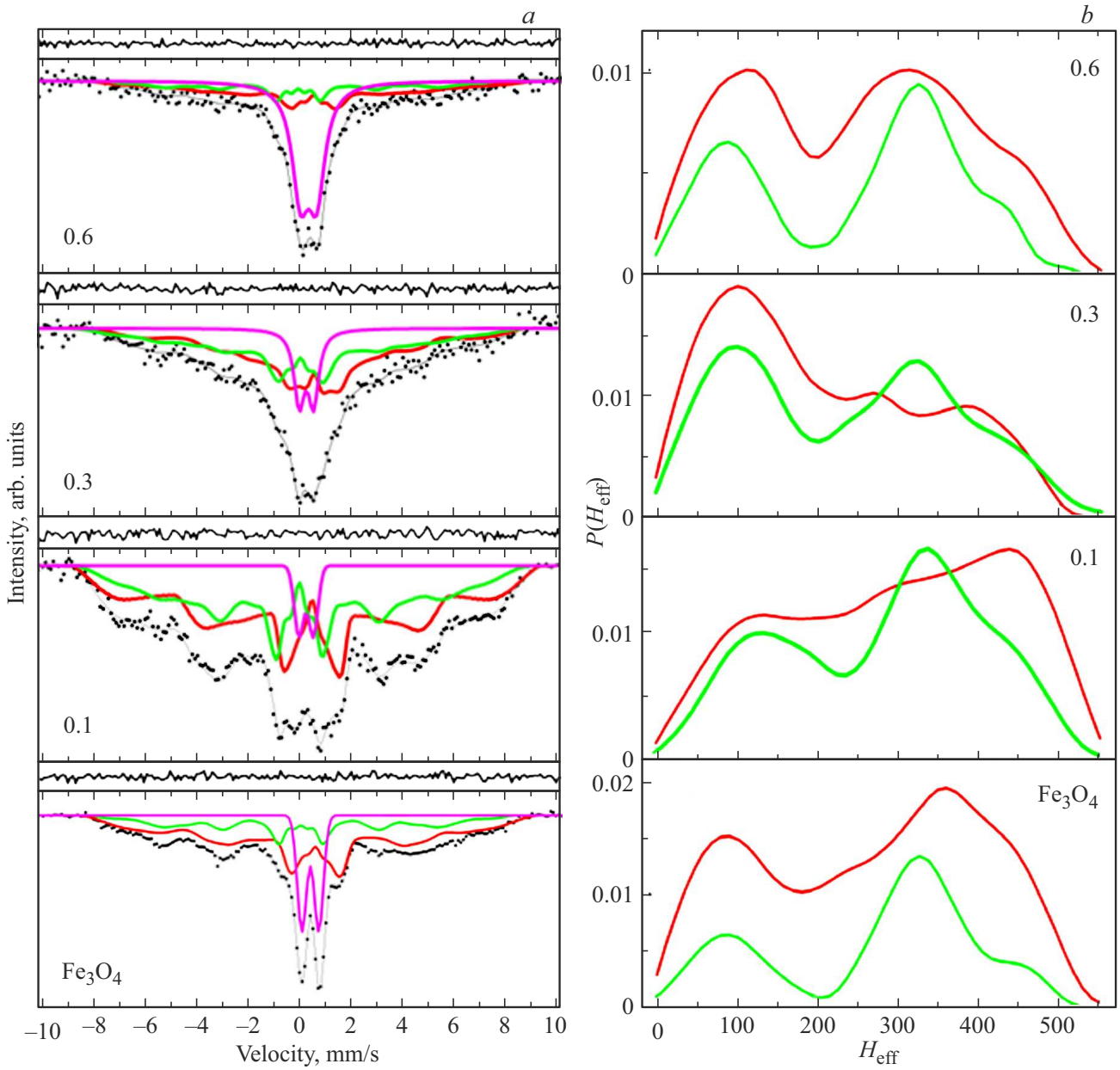

Figure 2. (a) Mössbauer spectra of the samples M/G0.0, M/G0.1, M/G0.3 and M/G0.6, obtained at 300 K, which are designated in the figures as Fe_3O_4, 0.1, 0.3 and 0.6, respectively, and (b) distributions of the effective magnetic fields, which are restored from the MS. The red lines belong to the ions Fe^{3+}, the green lines belong to the ions $Fe^{2.5+}$, and the crimson lines belong to doublets.

by the iron ions Fe^{3+} and Fe^{2+}, which occupy the A and B crystallographic positions. However, magnetite possesses a Verwey phase transition that is observed in the Fe_3O_4 bulk crystals at the temperature $T_V = 119$ K [22,49]. Within the temperatures above T_V, the iron ions Fe^{3+} and Fe^{2+} in the B-positions of the crystal lattice are in an ion-exchange state and they may be interpreted as cations $Fe^{2.5+}$ that are matched with one Zeeman sextuplet (ZS). As a result, at the temperatures above T_V the magnetite MS consists of two ZS.

The experimental MS that are mathematically processed by the software SpectrRelax [28] are shown in Figure 2, a and Figure 3, a, in which experimental values are dotted, while simulated components are marked with solid lines. Using the positions of the lines on the MS, we have calculated and analyzed HPI parameters, i. e. the line widths (G), the isomer shift (δ), the quadrupole splitting (ε), the effective magnetic field (H_{eff}) and intensities of the components (P), which are shown in Tables 3 and 4. The intensities of the lines (P) make it possible to specify a relative number of the iron ions in the non-equivalent positions and the phase states in the studied MNPs. Using the software [28], the experimental MS (Figure 2, a and Figure 3, a) were taken to calculate

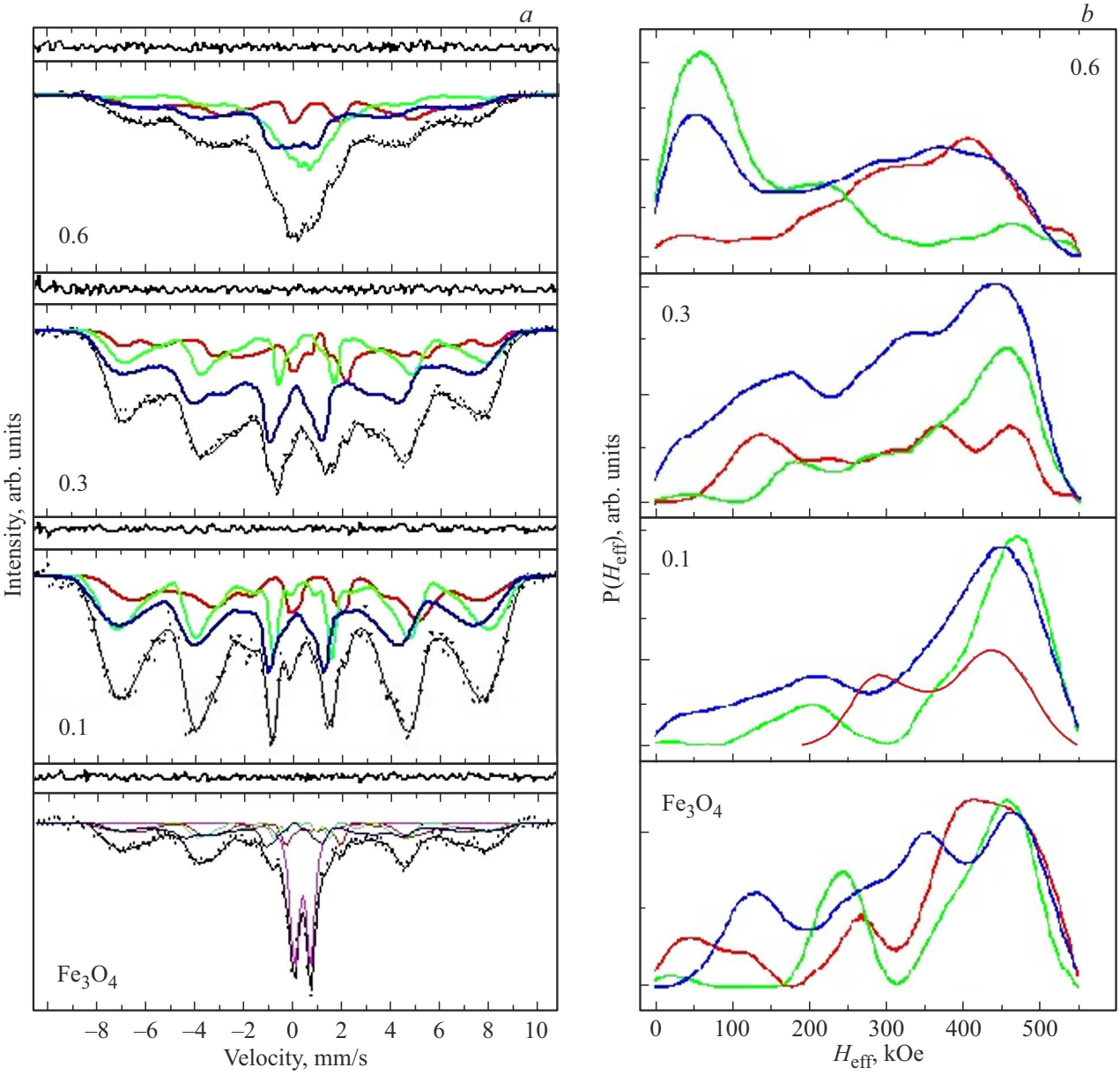

Figure 3. (a) Mössbauer spectra of the samples M/G0.0, M/G0.1, M/G0.3 and M/G0.6, which are obtained at 80 K, which are designated in the figure as Fe_3O_4, 0.1, 0.3 and 0.6, respectively, and (b) distributions of the effective magnetic fields, which are calculated therefrom. The blue lines belong to the ions Fe^{3+}, the green lines belong to the ions Fe^{2+}, the red lines belong to FeS, the crimson lines belong to a doublet.

functions of distribution of the effective magnetic fields $P(H_{\text{eff}})$, which are shown in Figure 2, b and Figure 3, b, respectively.

4.3. Mössbauer spectra of the MNPs, which are recorded at 300 K and their analysis

As it is clear in Figure 2, a, the room temperature MS consist of the Zeeman splitting wide lines, whose background exhibits doublets around the velocity zero. The doublet intensity increases with an increase of the glycine concentration in the sample.

Good agreement with the experimental room temperature MS was obtained when using the model that consisted of the two ZS belonging to the Fe ions in magnetite and a doublet.It is confirmed by minimality between the simulated and experimental values indicated above each spectrum (Figure 2, a) as well as values of χ^2 that are in the range 1.1–1.2.

As known, the IS values of the Fe ions in the A sites of the iron oxides are always less than those of the B ions in the B sites [22]. The HFI data were analyzed (Table 3) to show that the ZS (Figure 3, a) with the smaller IS value belongs to the ions Fe^{3+} in the A-positions, while another ZS with

Table 3. Parameters of hyperfine interactions, which are calculated from the room temperature Mössbauer spectra of the MNPs M/G0.0, M/G0.1, M/G0.3 and M/G0.6 (IS — the isomeric chemical shift, QS — the quadrupole splitting, H_{eff} — the effective magnetic field, P — the areas of the sextuplet or doublet)

Sample	Comp.		G, mm/s	IS, mm/s	QS, mm/s	H_{eff}, kOe	P, %
M/G0.6	Fe_3O_4	$Fe^{2.5+}$	0.210 ± 0.070	0.493 ± 0.080	-0.039 ± 0.080	248 ± 40	34 ± 13
		Fe^{3+}	0.210 ± 0.070	0.022 ± 0.120	0.077 ± 0.110	247 ± 50	19 ± 10
	Doublet		0.774 ± 0.090	0.343 ± 0.021	0.311 ± 0.013	–	47 ± 11
M/G0.3	Fe_3O_4	$Fe^{2.5+}$	0.301 ± 0.170	0.495 ± 0.130	-0.081 ± 0.110	208 ± 18	47 ± 14
		Fe^{3+}	0.301 ± 0.170	0.011 ± 0.110	-0.041 ± 0.090	234 ± 20	40 ± 16
	Doublet		0.476 ± 0.100	0.273 ± 0.040	0.274 ± 0.016	–	13 ± 5
M/G0.1	Fe_3O_4	$Fe^{2.5+}$	0.210 ± 0.040	0.395 ± 0.050	-0.119 ± 0.050	298 ± 13	55 ± 5
		Fe^{3+}	0.210 ± 0.040	0.061 ± 0.070	0.042 ± 0.060	281 ± 15	40 ± 4
	Doublet		0.431 ± 0.070	0.281 ± 0.040	0.274 ± 0.020	–	4 ± 2
Fe_3O_4	Fe_3O_4	$Fe^{2.5+}$	0.279 ± 0.190	0.427 ± 0.110	-0.132 ± 0.110	267 ± 20	60 ± 16
		Fe^{3+}	0.279 ± 0.190	0.001 ± 0.130	0.015 ± 0.120	326 ± 8	23 ± 16
	Doublet		0.430 ± 0.040	0.349 ± 0.016	0.321 ± 0.012	–	16 ± 5

Table 4. Parameters of hyperfine interactions, which are calculated from the Mössbauer spectra taken at 80 K for the MNPes M/G0.0, M/G0.1, M/G0.3 and M/G0.6 (IS — the isomeric chemical shift, QS — the quadrupole splitting, H_{eff} — the effective magnetic field, P — the areas of the sextuplet or doublet)

Sample	Comp.		G, mm/s	IS, mm/s	QS, mm/s	H_{eff}, kOe	P, %
M/G0.6	Fe_3O_4	Fe^{3+}	0.211 ± 0.240	0.108 ± 0.090	0.117 ± 0.080	244 ± 16	36 ± 15
		Fe^{2+}	0.208 ± 0.240	0.701 ± 0.090	-0.243 ± 0.090	332 ± 18	21 ± 14
		FeS	0.209 ± 0.130	0.412 ± 0.070	-0.042 ± 0.080	150 ± 21	42 ± 21
M/G0.3	Fe_3O_4	Fe^{3+}	0.226 ± 0.080	0.513 ± 0.080	-0.030 ± 0.070	376 ± 14	27 ± 19
		Fe^{2+}	0.227 ± 0.080	0.801 ± 0.130	-0.273 ± 0.130	311 ± 14	23 ± 12
		FeS	0.228 ± 0.080	0.154 ± 0.040	0.044 ± 0.035	282 ± 19	50 ± 14
M/G0.1	Fe_3O_4	Fe^{3+}	0.246 ± 0.320	0.428 ± 0.100	0.000 ± 0.070	408 ± 15	31 ± 5
		Fe^{2+}	0.249 ± 0.600	0.800 ± 0.190	-0.241 ± 0.190	383 ± 10	20 ± 17
		FeS	0.248 ± 0.340	0.183 ± 0.120	0.007 ± 0.110	346 ± 16	49 ± 31
Fe_3O_4	Fe_3O_4	Fe^{3+}	0.200 ± 0.240	0.409 ± 0.120	0.030 ± 0.130	378 ± 13	18 ± 50
		Fe^{2+}	0.200 ± 0.240	0.625 ± 0.140	-0.257 ± 0.140	363 ± 40	24 ± 24
		FeS	0.220 ± 0.400	0.326 ± 0.210	0.243 ± 0.210	335 ± 39	29 ± 40
	Doublet		0.390 ± 0.070	0.412 ± 0.016	0.329 ± 0.023	–	29 ± 10

the higher IS value belongs to the ions Fe^{3+} and Fe^{2+} that occupy the B sites. The room temperature MS of the Fe_3O_4 MNPs (Figure 2, *a* and 3, *a*) is different from a bulk magnetite spectrum that is unavailable herein, but similar to one provided in the studies [50–52]. The room temperature MS of the Fe_3O_4 macroscopic crystal consists of two sextuplets [50–52], wherein one of them belongs to the ions Fe^{3+} and the other belongs to the mixed ions Fe^{2+} and Fe^{3+}.

The MS of the particles (Figure 2, *a*) exhibit doublets against the background of the ZS wide lines. The sextuplets observed in Figure 2, *a* indicate certain magnetic ordering

in the particles, while the width of these lines means size distribution of the particles. Magnetite crystallizes in the cubic structure, for which quadrupole splitting is zero. Consequently, QS near-zero values of the sextuplets belonging to the ions Fe^{3+} and $Fe^{2.5+}$ (Table 3) indicate that these ions are arranged within the volume of the particles. The quadrupole splitting doublets on the MS (Figure 2, *a*) mean that cubic symmetry is disturbed. This disturbance is caused by a surface that forms a non-zero gradient of an electric field that creates quadrupole splitting. It should be noted that with an increase of the glycine concentration the particle sizes decrease, thereby resulting in an increase of a surface/volume ratio, an increase of the relative number of the ions in the surface layer and, therefore, and an increase of the doublet line intensity (Table 3).

As it is clear from Table 3, the values of H_{eff} decrease with the increase of the glycine concentration, thereby indicating the decrease of the particle size, which agrees with X-ray diffraction data (Table 1).

4.4. Mössbauer spectra of the MNPs, which are recorded at 80 K and their analysis

At the temperatures below T_V, the experimental MS of the magnetite MNPs significantly change [29,30,36,48,53] and MS interpretation is significantly complicated. For this reason, the MS interpretations are quite contradictory. Results of the low-temperature Mössbauer studies [54–59] as well as nuclear magnetic resonance [60,61] indicate against validity of the Verwey description [62] that implies existence of the three components. It is due to the fact that at the temperatures below T_V electron exchange does not exist and only one for each of the three types of atoms is observed (in the tetra-positions Fe^{3+} and two in the octa-positions Fe^{2+}, Fe^{3+}). Thus, an adequate model for description of the magnetite MS has not been found yet. Data interpretation is difficult since direct structure information about properties of a dielectric state of the magnetite crystals is almost unavailable because of twinning.

The MS obtained at the temperature of 80 K were described using various models, namely, consisting of one doublet and five, four or three ZS. As a result, it was found that the experimental MS of the Fe_3O_4 MNPs are best described by superposition of the three ZS and one doublet, so are the MS of the Fe_3O_4 MNPs with glycine by means of the three ZS, which is confirmed by minimal values of a difference between the simulated and experimental values as well as by values of χ^2 within 1.1–1.2. The HFI parameters calculated from the MS are shown in Table 4.

The MS reliably identifies the spectral lines belonging to the ions Fe^{2+} and Fe^{3+} by their chemical shifts that are $\sim 0.2-0.5$ mm/s for Fe^{3+} and $\sim 0.9-1.1$ mm/s for Fe^{2+} [11]. In case of the spinel ferrite MNPs, the IS values belonging to the iron ions in the high-spin state Fe^{3+} are usually within 0.3–0.6 mm/s [63], whereas there are no values of the chemical shifts (from 0.9 to 1.1 mm/s), which belong to the Fe ions in the low-spin state Fe_3O_4. As it is clear from Table 2, the IS values are within 0.3–0.5 mm/s. It means that the studied MNPs (Figure 3, *a*) exhibit the iron ions in the high-spin state Fe^{3+}.

In the MS, compliance of the ZS to the tetra- (A) and octa- (B) ions of Fe was found based on IS values of the chemical shifts [18]. The ZS (Figure 4, *a*) with the smaller IS value belongs to the ions Fe^{3+} in the tetra-positions, while the ZS with the higher IS values belongs to the ions of Fe (Fe^{3+} and Fe^{2+}), which occupy the octa-sites.

In case of the Fe_3O_4 MNPs, the doublet line intensity in the MS at 80 K is almost in two times higher than for the doublets of these particles at the room temperature. The doublet line intensities are reduced in such a degree since a blocking point is below the room temperature and therefore the ZS is formed.

Let us consider the causes of formation of the MS of the MNPs of the sextuplet FeS (Figure 3). It can be assumed that this ZS belongs to a secondary phase, as, for example, α-FeOOH [64], which is formed during synthesis of the samples. However, X-ray diffraction data do not show the secondary phases, impurities or amorphous forms in the studied MNPs. In some studies, the ZS that has the least effective fields is attributed to the ions Fe^{2+}, which occupy the octa-positions [54–59].

As discussed above, the doublets observed on the room temperature MS (Figure 2) occur due to disturbance of a surrounding of the Fe ions by such a defect as a surface. It can be assumed that this disturbance of the surrounding of the Fe ions by presence of the surface results in formation of the FeS line. Thus, the FeS lines belong to the Fe ions that are arranged in the surface layer and lost a part of the nearest magnetic neighbors due to the surface. It is clear from Table 4 that with the increase of the glycine concentration resulting in reduction of the particle sizes, significant reduction of the effective field of the ZS of the FeS ions is observed. The MNP surface layer with canting magnetic structure (CMS), which is also referred to as a „magnetically dead“ layer, results in a significant change of the magnetic properties of the particles.

Existence of an anisotropic layer on a surface of ferromagnetic crystals was theoretically predicted by L. Néel in 1954 [65]. Experimental studies of the structure and the properties of the surface layer attracted attention much later (see [66,67] and references therein). Existence of the surface layer with the CMS in the MNPs was assumed based on magnetic measurements in the study [68]. Based on the Mössbauer measurements in the strong magnetic fields [69], it was assumed that the CMS existed on the MNP surface. However, an attribution of the canting structure to the particle surface or the volume of the particle is still discussed. Many Mössbauer studies are dedicated to investigation of the particle surface, but causes of formation of these spectra were explained differently, wherein the surface layer with CMS was not involved (see [22] and references therein). It was assumed, for example, that the ZS with the high line widths and the significantly smaller effective fields belonged to the iron ions arranged in the

MNP surface layer, but no arguments were given to support this assumption [36,49,70–73].

Proofs of existence of the surface CMS on the surface could have been obtained when directly comparing properties of the surface and volume of the particles or crystals. It was enabled by a new unique method „Simultaneous Gamma, X-ray and Electron Mössbauer Spectroscopy (SGXEMS)", which was proposed and realized for the first time in the study [74–76]. The SGXEMS method is unique in that information about the properties of the surface layer and the volume of the crystal is simultaneously extracted, wherein the same method (the Mössbauer effect) is used, thereby allowing directly comparing experimental data on the state of the surface and volume of the crystal. The SGXEMS method was used to obtain the first proofs that the surface has the Fe_3BO_6 macroscopic crystals as well as the hexagonal ferrites $BaFe_{12}O_{19}$ and $SrFe_{12}O_{19}$ doped with diamagnetic ions [77–83] of a „transitional" (in the terminology of that time) layer (or a „canting structure" in the modern terminology). Introduction of diamagnetic ions results in additional disruption of superexchange bonds and an increase of the thickness of the CMS layer [80–83]. Within the „transitional" layer, orientation of magnetic moments of the iron ions (as approaching the surface) smoothly deviates from a direction in the volume [77,78]. The MS of the $MFe_{12}O_{19}$ ferrites were analyzed to show that the thickness of the transitional layer in these crystals did not exceed several nm [83], which agrees with the Néel calculations [65]. The surface layer with CMS, which is detected in the magnetic macrocrystals, can be maintained when the crystallite size decreases to the nanoscale [77–83]. Later the SGXEMS method in foreign literature was called „Simultaneous Triple Radiation Mossbauer Spectroscopy (STRMS)" [84,85]. It is important to detect the surface layer with CMS in the MNPs because this layer results in the change of the magnetic properties of the particles, in particular, in reduction of saturation magnetization of the MNPs [32].

Thus, the obtained results confirm conclusions of the studies [22,87], in which it was shown for the first time without using the high magnetic fields (costly equipment) that the canting structure of the magnetic moments was observed exactly in the surface layer of the SF MNPs.

4.5. Functions of distribution of the effective magnetic fields $P(H_{\text{eff}})$ in the studied MNPs

No resolution of the MS ZS of the studied MNPs significantly complicates obtaining of a specific physical model that describes the spectra. The function of distribution of the effective magnetic fields $P(H_{\text{eff}})$ turns out to be convenient for studying the properties of the materials due to high sensitivity of the field H_{eff} to the nearest surrounding of the ion ^{57}Fe. The software [28] also allows restoring the functions $P(H_{\text{eff}})$ shown in Figures 2, *b* and 3, *b* from the MS. The best agreement with the experimental room temperature spectra was obtained when using two functions of distributions H_{eff}, whereas for the MS at 80 K — the three functions $P(H_{\text{eff}})$ As it is clear from Figure 2, *b*, the functions $P(H_{\text{eff}})$ consist of the two curves and the paramagnetic phase, whose forms are different from the functions $P(H_{\text{eff}})$ for the magnetite macrocrystal (not shown here), which exhibits maximums that correspond only to the two effective fields 489 and 460 kOe, which agrees with the data of the studies [50–52].

The functions $P(H_{\text{eff}})$ obtained from the room temperature MS (Figure 2, *a*) exhibit maximum in the two ranges of H_{eff}: from 50 to 250 kOe and from 250 to 550 kOe. It may mean that the synthesized particles are divided by sizes into two groups, namely, in the range of at most 6 nm, which correspond to the maximum at H_{eff} (Figure 2, *b*) within the range from 50 to 250 kOe. The second maximum at H_{eff} (Figure 2, *b*) within the range from 200 to 550 kOe indicates existence of the MNPs of the sizes ≈ 8 nm. The increase of the glycine concentration results in an increase of intensity of the lines on the functions $P(H_{\text{eff}})$ within the range 50−200 kOe and reduction of intensity of the peak within the range 200−500 kOe. It can be explained by two methods. One of them is that the increase of the glycine concentration results in an increase of isolation of the particles from each other and, therefore, a decrease of magnetic interactions between the particles. The increase of the amount of glycine during synthesis results in acceleration and termination of the synthesis process before formation of the larger particles, i. e. the smaller-size particles are synthesized and superparamagnetic effects are enhanced.

The restored from the MS obtained at 80 K (Figure 3, *b*) consist of the three distribution curves of distribution H_{eff}, wherein two of them behave almost identically and do not depend on the synthesis conditions. The isomer shifts of one ZS are much higher than in the other, thereby making it possible to attribute these ZS (Table 4) as well as the functions of distribution to the B- and A-sublattices, respectively.

Let us consider causes of differences of the functions of distribution H_{eff} of the MNPs and the macrocrystals. First of all, presence of the surface results in reduction of the number of the exchange bonds of the iron ions arranged on the surface. Therefore, in case of the MNPs, the contribution to the MS by the Fe ions of the surface layer increases, i. e. a „surface factor" becomes significant. The maximum on the function $P(H_{\text{eff}})$ around 350 kOe can be related to the ions of the surface layer. At the same time, the maximum around 480 kOe on the distributions $P(H_{\text{eff}})$ (Figures 2, *b* and 3, *b*) belongs to the iron ions arranged within the MNP volume.

The behavior of the third function of distribution H_{eff}, which is observed in Figure 3, *b*, can be also explained by the fact that during synthesis a core-shell structure is formed in the MNPs Fe_3O_4 and Fe_3O_4@Gl and its core is magnetite surrounded by a shell of the oxidized layer that is similar to maghemite. The thickness of this surface layer is very small and sensitivity of the X-ray diffraction method and the

Mössbauer effect will be insufficient to specify the phase attribution of this surface layer. It should be noted that the above-given interpretation of the Mössbauer data agrees with existing representations of the magnetism theory.

4.6. Size estimation of the synthesized MNPs Fe_3O_4 and Fe_3O_4@Gly

The Mössbauer spectroscopy is very sensitive to sizes of the studies particles. By comparing the MSe with the MS of the particles, whose sizes are directly specified, one can estimate the sizes of the studied MNPs. Thus, in case of the MNPs of the sizes of several nm, a velocity of relaxation of the magnetization vector exceeds a speed of Larmor precession of a nuclear spin. As a result, the average value of hyperfine interactions becomes zero and the MS exhibits a quadrupole doublet or singlet. If the particle size ranges from 6 to 10 nm, then the MS consists of the wide Zeeman splitting lines, whose background exhibits the quadrupole doublet or singlet. With an increase of the size of the studied MNPs to 10−12 nm, the MS are transformed into the ZS with the quite wide lines, whose resolution is absent. The increase of the particle size 20 nm results in differences of the ZS of the various phases or states of the Fe ions.

Thus, the Mossbauer spectroscopy method was used to study the Fe_3O_4 MNPs of the sizes from 3 to 20 nm [22,23,34–36,42–48,88–92]. It was shown that if the sizes of the Fe_3O_4 MNPs are 7 nm or less, then the MS exhibits only the doublet [88,90]. With the sizes of the Fe_3O_4 MNPs, which exceed 10 nm, the MS consists of the ZS with the high line widths [92]. The obtained MS are analyzed and compared with published studies, so it is fair to say that the sizes of the Fe_3O_4 MNPs are 8 nm. The increase of the amount of glycine during synthesis of the MNPs M/G0.1, M/G0.3 and M/G0.6 results in reduction of the MNP sizes, namely, 11, 10 and 6 nm, respectively.

5. Conclusions

The properties, the phase composition and the magnetic structure of the glycine-modified iron oxide nanoparticles (Gl) have been systematically studied. The particles are synthesized by the glycine-modified method by adjusting an MNP oxidation time. Based on the experimental X-ray diffraction and Mössbauer data, it is found that the MNPs synthesized with the various glycine concentration degree are magnetite (Fe_3O_4) and do not contain impurities of the other phase. Based on analysis of the hyperfine interactions parameters calculated from the Mössbauer spectra and the functions of distribution of the effective magnetic fields $P(H_{\text{eff}})$ of the MNPs Fe_3O_4 and Fe_3O_4@Gl, it is found that the structure of the spin magnetic moment in the surface layer of the studied MNPs is different from a collinear structure within the volume of the particles. Causes of formation of the this MNP magnetic structure significantly affecting the properties of the particles are discussed.

The results obtained in the study pave new ways for creating materials based on controllable surface spin ordering, which is important for applying the nanomagnetics in biomedicine for diagnostics and therapy of human diseases.

Conflict of interest

The authors declare that they have no conflict of interest.

References

[1] Ferrites and Ferrates: Chemistry and Applications in Sustainable Energy and Environmental Remediation. Ed-s. V.K. Sharma, R. Doong, H. Kim, R.S. Varma, D.D. Dionysiou. ACS Symposium Series; Volume American Chemical Society: Washington, DC, 2016. DOI: 10.1021/bk-2016-1238.
[2] E.V. Tomina, B.V. Sladkopevtsev, N.A. Tien, V.Q. Mai. Inorganic Mater., **59**, *13*, 1363 (2023). DOI: 10.1134/S0020168523130010.
[3] Nanoparticles for Biomedical Applications: Fundamental Concepts, Biological Interactions and Clinical Applications. Ed. E.J. Chung, L. Leon, C. Rinaldi. Elsevier (2019). 440 p.
[4] Hybrid Nanostructures for Cancer Theranostics. Ed. R.A. Bohara, N. Thorat. Elsevier Inc. (2019). 424 p.
[5] F. Fabris, E. Lima, Jr.E. De Biasi, H.E. Troiani, M.V. Mansilla, T.E. Torres, R.F. Pacheco, M.R. Ibarra, G.F. Goya, R.D. Zysler, E.L. Winkler. Nanoscale **11**, 3164 (2019).
[6] I.M. Obaidat, V. Narayanaswamy, S. Alaabed, S. Sambasivam, C.V.V.M. Gopi. Magnetochemistry **5**, 67 (2019). https://doi.org/10.3390/magnetochemistry5040067
[7] R.K. Gilchrist, R. Medal, W.D. Shorey, R.C. Hanselman, J.C. Parrott, C.B. Taylor. Ann. Surg. **146**, 596 (1957).
[8] M.R. Ghazanfari, M. Kashefi, S.F. Shams, M.R. Jaafari. Biochemistry Research International.Volume 2016, Article ID 7840161.
[9] B. Gleich, J. Weizenecker. Nature. **435**, 1214 (2005). https://doi.org/10.1038/nature03808
[10] Gleich, J. Weizenecker, H. Timminger, C. Bontus, I. Schmale, J. Rahmer, J. Schmidt, J. Kanzenbach, J. Borgert, in Proc. ISMRM, **18**, 1920 (2010).
[11] A.S. Kamzin, N. Dogan, L.S. Kamzina, A.V. Kopylov. FTT, **67**, *2*, 356 (2025). (in Russian). DOI: 10.61011/FTT.2025.02.59992.29-25.
[12] N. Dogan, O.M. Dogan, M. Irfan, F. Ozel, A.S. Kamzin, V.G. Semenov, I.V. Buryanenko. J. Magn. Magn. Mater. **561**, 169654 (2022). https://doi.org/10.1016/j.jmmm.2022.169654
[13] A.S. Kamzin, G. Caliskan, N. Dogan, A. Bingolbali, V.G. Semenov, I.V. Buryanenko. Phys. Sol. State, **64**, *10*, 1550 (2022). DOI: 10.21883/PSS.2022.10.54249.391
[14] N. Dogan, G. Caliskan, M. Irfan. J. Mater. Sci.: Mater. Electron. **34**, 390 (2023). https://doi.org/10.1007/s10854-022-09799-x.
[15] W. Li, X. Jia, L. Yin, Z. Yang, H. Hui, J. Li, W. Huang, J. Tian, S. Zhang. iLIVER **1**, 237 (2022). https://doi.org/10.1016/j.iliver.2022.10.003.
[16] B.A. Zasonska, V.I. Patsula, R. Stoika, D. Horák. Surface-Modified Magnetic Nanoparticles for Cell Labeling. In Book „Process Advancement in Chemistry and Chemical Engineering Research". Ch. 17, p. 275. 2016 Academic Press. https://doi.org/10.1201/b19839

[17] S. Liu, B. Yu, S. Wang, Y. Shen, H. Cong. Adv. Colloid Interface Sci. **281**, 102165 (2020). https://doi.org/10.1016/j.cis.2020.102165.
[18] A.S. Kamzin, N. Dogan, O.M. Dogan, V.G. Semenov. Phys. Solid State, **65**, *8*, 1373 (2023). DOI: 10.21883/PSS.2023.08.56587.127
[19] A.S. Kamzin, V.G. Semenov, L.S. Kamzina. Phys. Solid State, **66**, *7*, 1183 (2024). DOI: 10.61011/PSS.2024.07.58996.74
[20] A. Omelyanchik, A.S. Kamzin, A.A. Valiullin, V.G. Semenov, S.N. Vereshchagin, M. Volochaev, A. Dubrovskiy, I. Kozenkov, E. Dolan, D. Peddis, A. Sokolov, V. Rodionova. Colloids and Surfaces A: Physicochemical and Engineering Aspects **647**, 129090 (2022). https://doi.org/10.1016/j.colsurfa.2022.129090.
[21] S. Mørup, M.F. Hansen, C. Frandsen. Magnetic Nanoparticles. 2-nd Ed. Elsevier Inc. (2018). DOI: 10.1016/B978-0-12-803581-8.11338-4
[22] A.S. Kamzin, I.M. Obaidat, A.A. Valliulin, V.G. Semenov, I.A. Al-Omari. Phys. Solid State **62**, 1933 (2020), doi.org/10.1134/S1063783420100157.
[23] A.S. Kamzin, I.M. Obaidat, V.G. Semenov, V. Narayanaswamy, I.A. Al-Omari, B. Issa, I.V. Buryanenko. Phys. Solid State **65**, *3*, 470 (2023). DOI: 10.21883/PSS.2023.03.55591.544.
[24] D.N. Belysheva, O.Yu. Sinel'shchikova, N.G. Tyurnina, Z.G. Tyurnina, S.I. Sviridov, A.V. Tumarkin, M.V. Zlygostov, V.L. Ugolkov. FTT **61**, *12*, 2364 (2019). (in Russian). DOI: 10.21883/FTT.2019.12.48555.11ks
[25] E.V. Mashkovtseva, N.A. Rudnikova, V.S. Kopylova, Y.R. Nartsissov. Pharmacy & Pharmacology. **12**, *3*, 198 (2024). DOI: 10.19163/2307-9266-2024-12-3-198-208
[26] C. Pereira, A.M. Pereira, C. Fernandes, M. Rocha, R. Mendes, M.P. Fernández-García, A. Guedes, P.B. Tavares, J.M. Grenéche, J.P. Araújo, C. Freire. Chem. Mater. **24**, 1496 (2012), https://doi.org/10.1021/cm300301c.
[27] E.V. Shelekhov, T.A. Sviridova. Met. Sci. Heat Treat. **42**, 309 (2000), https://doi.org/10.1007/BF02471306.
[28] M.E. Matsnev, V.S. Rusakov. AIP Conf. Proc. **1489**, 178 (2012), https://doi.org/10.1063/1.4759488.
[29] T.J. Daou, G. Pourroy, S. Bégin-Colin, J.M. Grenéche, C. Ulhaq-Bouillet, P. Legaré, P. Bernhardt, C. Leuvrey, G. Rogez. Chem. Mater. **18**, 4399 (2006). https://doi.org/10.1021/cm060805r
[30] A. Demortiére, P. Panissod, B.P. Pichon, G. Pourroy, D. Guillon, B. Donnio, S. Bégin-Colin. Nanoscale. **3**, 225 (2011). DOI: 10.1039/c0nr00521e.
[31] S.H. Gee, Y.K. Hong, D.W. Erickson, M.H. Park, J.C. Sur. J. Appl. Phys. **93**, 7560 (2003). doi: 10.1063/1.1540177.
[32] Z. Shaterabadi, G. Nabiyouni, G.F. Goya, M. Soleymani. Applied Phys. **A128**, 631 (2022). https://doi.org/10.1007/s00339-022-05675-x.
[33] A. Omelyanchik, F.G. da Silva, G. Gomide, I. Kozenkov, J. Depeyrot, R. Aquino, A.F.C. Campos, D. Fiorani, D. Peddis, V. Rodionova, S. Jovanović. J. Alloy. Compd. **883**, 160779 (2021). https://doi.org/10.1016/j.jallcom.2021.160779.
[34] A.G. Akopdzhanov, N.L. Shimanovskii, V.Yu. Naumenko, I.P. Suzdalev, V.K. Imshennik, Yu.V. Maksimov, S.V. Novichikhin, Russian J. Phys. Chem. B **8**, 584 (2014)
[35] D.K. Kim, M. Mikhaylova, Y. Zhang, M. Muhammed. Chem. Mater. **15**, 1617 (2003).
[36] Z. Surowiec, M. Budzyński, A. Miaskowski. Nukleonika **62**, 183 (2017). doi: 10.1515/nuka-2017-0028.
[37] J.B. Mamania, L.F. Gamarra, G.E. de S. Brito. Materials Research. **17**, 542 (2014)
[38] P.B. Rathod, A.K. Pandey, S.S. Meena, A.A. Athawale. RSC Advan. **6**, 21317 (2016). https://doi.org/10.1039/C6RA01543C.
[39] G.M. da Costa, E. De Grave, R.E. Vandenberghe. Hyperfine Interact. **117**, 207 (1998). https://doi.org/10.1023/A:1012691209853.
[40] N. Joumaa, P. Toussay, M. Lansalot, A. Elaissari. J. Polymer Sci.: Part A: Polymer Chem. **46**, 327 (2008). DOI: 10.1002/pola.22383.
[41] G.F. Goya, T.S. Berquo, F.C. Fonseca, M.P. Morales. J. Appl. Phys. **94**, *5*, 3520 (2003). DOI: 10.1063/1.1599959.
[42] H. Topsoe, J.A. Dumesic, M. Boudart. J. de Phys. Col. C6, suppl N 12, 35, C6-411 (1974). http://dx.doi.org/10.1051/jphyscol:1974680.
[43] V.V. Grecu, S. Constantinescu, M.N. Grecu, R. Olar, M. Badea, R. Turcu. Hyperfine Interact. **183**, 205 (2008). DOI: 10.1007/s10751-008-9753-2.
[44] V. Kuncser, G. Schinteie, R. Alexandrescu, I. Morjan, L. Vekas, G. Filoti. Magnetic Configuration and Relaxation in Iron Based Nano-Particles: A Mössbauer Approach. In: Bârsan V., Aldea A. (eds) Trends in Nanophysics. Engineering Materials. Springer, Berlin, Heidelberg (2010). https://doi.org/10.1007/978-3-642-12070-1_13.
[45] A.F.R. Rodriguez, T.P. Costa, R.A. Bini, F.S.E.D.V. Faria, R.B. Azevedo, M. Jafelicci Jr., J.A.H. Coaquira, M.A.R. Martínez, J.C. Mantilla, R.F.C. Marques, P.C. Morais. Physica B **521**, 141 (2017). http://dx.doi.org/10.1016/j.physb.2017.06.043.
[46] V.A.J. Silva, P.L. Andrade, A. Bustamante, L. de l.S. Valladares, M. Mejia, I.A. Souza, K.P.S. Cavalcanti, M.P.C. Silva, J.A. Aguiar. DOI: 10.1007/s10751-013-0875-9.
[47] A. Mitra, J. Mohapatra, S.S. Meena, C.V. Tomy, M. Aslam. J. Phys. Chem. C **118**, 19356 (2014). dx.doi.org/10.1021/jp501652e.
[48] S.S. Pati, L.H. Singh, E.M. Guimaraes, J. Mantilla, J.A.H. Coaquira, A.C. Oliveira, V.K. Sharma, V.K. Garg. J. All. Comp. **684**, 68 (2016). http://dx.doi.org/10.1016/j.jallcom.2016.05.160.
[49] Ya. Smit, Kh. Vein. Ferrity. Izd-vo IL, M. (1962). 504 s. (in Russian).
[50] F.J. Berry, S. Skinner, M.F. Thomas, J. Phys. Condens. Matter **10**, 215 (1998).
[51] C.E. Johnson, J.A. Johnson, H.Y. Hah, M. Cole, S. Gray, V. Kolesnichenko, P. Kucheryavy, G. Goloverda. Hyperfine Interact. **237**, 27 (2016). DOI: 10.1007/s10751-016-1277-6.
[52] A.I. Nikiphorov, E.O. Lazareva, E.V. Edemskaya, V.G. Semenov, K.G. Gareev, D.V. Korolev. Kolloidnyi zhurnal. **86**, 469 (2024). DOI: 10.31857/S0023291224040062.
[53] F. van der Woude, G.A. Sawatzky, A.H. Morrish. Phys. Rev **167**, 533 (1968).
[54] B.J. Evans, S.S. Hafner. J. Appl. Phys. **40**, 1411 (1969).
[55] R.S. Hargrove, W. Kündig. Solid State Commun. **8**, 303 (1970). https://doi.org/10.1016/0038-1098(70)90455-2.
[56] M. Rubinstein, D.W. Forester. Solid State Commun. **9**, 1675 (1971). https://doi.org/10.1016/0038-1098(71)90339-5.
[57] J. García, G. Subías. J. Phys.: Condens. Matter **16**, R145 (2004). DOI: 10.1088/0953-8984/16/7/R01.
[58] I. Dézsi, Cs. Fetzer, Á. Gombköto, I. Szucs, J. Gubicza, T. Ungár. J. Appl. Phys. **103**, 104312 (2008).

[59] R. Reznícek, V. Chlan, H. Štepánková, P. Novák, J. Zukrowski, A. Kozłowski, Z. Kakol, Z. Tarnawski, J.M. Honig. Phys. Rev. B **96**, 195124 (2017)
[60] M.S. Senn, J.P. Wright, J.P. Attfield. Nature (London) **481**, 173 (2012).
[61] M. Mizoguchi, M. Inoue. J. Phys. Soc. Jpn. **70**, 2333 (2001).
[62] E.J.W. Verwey, W. Haayman, F.C. Romeijin. J. Chem. Phys. **15**, 18L (1947).
[63] A.S. Kamzin, G. Caliskan, N. Dogan, A. Bingolbali, V.G. Semenov, I.V. Buryanenko. Phys. Solid State **64**, *10*, 1550 (2022). DOI: 10.21883/PSS.2022.10.54249.391
[64] D.F. Valezi, M.T. Piccinato, P.W.C. Sarvezuk, F.F. Ivashita, A. Paesano Jr., J. Varalda, D.H. Mosca, A. Urbano, C.L.B. Guedes, E. Di Mauro. Mater Chem Phys. **173**, 179 (2016). doi:10.1016/j.matchemphys.2016.01.067
[65] L. Neel. J. Physique **15**, *4*, 225 (1954).
[66] A.S. Kamzin, L.A. Grigor'ev. JETP Lett. **57**, *9*, 557 (1993).
[67] A.S. Kamzin, L.A. Grigor'ev. ZETP **77**, *4*, 658 (1993).
[68] R.H. Kodama, A.E. Berkowitz, E.J. McNiff, S. Foner. Phys. Rev. Lett. **77**, 394 (1996).
[69] J.M.D. Coey. Phys. Rev. Lett. **27**, *17*, 1140 (1971). doi:10.1103/PhysRevLett.27.1140.
[70] V. Sepelak, D. Baabe, F.J. Litterst, K.D. Becker. J. Appl. Phys. **88**, *10*, 5884 (2000). DOI: 10.1063/1.1316048
[71] F. Marquez-Linares, O.N.C. Uwakweh, N. Lopez, E. Chavez, R. Polanco, C. Morant, J.M. Sanz, Elizalde, C. Neira, S. Nieto, R. Roque-Malherbe. Journal of Solid State Chemistry **184**, 655 (2011). doi:10.1016/j.jssc.2011.01.017.
[72] I.S. Lyubutin, S.S. Starchikov, T.V. Bukreeva, I.A. Lysenko, S.N. Sulyanov, N.Y. Korotkov, S.S. Rumyantseva, I.V. Marchenko, K.O. Funtov, A.L. Vasiliev. Mater. Sci. Eng. C **45**, 225 (2014). https://doi.org/10.1016/j.msec.2014.09.017
[73] I.S. Lyubutin, S.S. Starchikov, L. Chun-Rong, N.E. Gervits, N.Y. Korotkov, T.V. Bukreeva. Croat. Chem. Acta **88**, 397 (2015). https://doi.org/10.5562/cca2739
[74] A.S. Kamzin, V.P. Rusakov, L.A. Grigoriev. Int. Conf. USSR. Proc. Part II, 271 (1988).
[75] A.S. Kamzin, L.A. Grigor'ev. Sov. Tech. Phys. Lett. **6**, *6*, 417(1990).
[76] A.S. Kamzin, L.A. Grigor'ev. Sov. Tech. Phys. **35**, *7*, 840 (1990).
[77] A.S. Kamzin, L.A. Grigor'ev. JETP Lett. **57**, *9*, 557 (1993).
[78] A.S. Kamzin, L.A. Grigor'ev. ZETP **77**, *4*, 658 (1993).
[79] A.S. Kamzin. JETP **89**, *5*, 891 (1999).
[80] A.S. Kamzin, L.P. Ol'khovik, V.L. Rozenbaum. Phys. Solid State **41**, *3*, 433 (1999).
[81] A.S. Kamzin, V.L. Rozenbaum, L.P. Ol'khovik. JETP Lett. **67**, *10*, 843 (1998).
[82] A.S. Kamzin, L.P. Ol'khovik. FTT **41**, *10*, 1806 (1999). (in Russian).
[83] A.S. Kamzin, L.P. Ol'khovik, V.L. Rozenbaum. JETP **84**, *4*, 788 (1997).
[84] F. Schaaf, U. Gonser. Hyperfine Interact. **57**, *1–4*, 2101 (1990).
[85] U. Gonzer, P. Schaaf, F. Aubertin. Hyperfine Interact. **66**, *1–4*, 95 (1991).
[86] A.E. Berkowitz, W.J. Schuele. J. Appl. Phys. 1959; 30: S134.
[87] A.S. Kamzin, G. Caliskan, N. Dogan, A. Bingolbali, V.G. Semenov, I.V. Buryanenko. Phys. Solid State **64**, *10*, 1550 (2022). DOI: 10.21883/PSS.2022.10.54249.391
[88] E.S. Vasil'eva, O.V. Tolochko, V.G. Semenov, V.S. Volodin, D. Kim. Tech. Phys. Letta. **33**, 40 (2007). https://doi.org/10.1134/S1063785007010117.
[89] A.F. Lehlooh, S.H. Mahmood. J. Magn. Magn. Mater. **151**, 163 (1995), https://doi.org/10.1016/0304-8853(95)00385-1.
[90] Z. Surowiec, M. Budzýnski, K. Durak, G. Czernel. Nukleonika **62**, 73 (2017). https://doi.org/10.1515/nuka-2017-0009.
[91] P. Burnham, N. Dollahon, C.H. Li, A.J. Viescas, G.C. Papaefthymiou. J. Nanopart. **2013**, 1 (2013), https://doi.org/10.1155/2013/181820.
[92] R.R. Gabbasov, V.M. Cherepanov, M.A. Chuev, M.A. Polikarpov, V.Y. Panchenko. Hyperfine Inter. **226**, 383 (2014), https://doi.org/10.1007/s10751-013-0960-0.

Translated by M.Shevelev